Polymer 205 (2020) 122857

Contents lists available at ScienceDirect

Polymer

journal homepage: http://www.elsevier.com/locate/polymer

Hypercrosslinked porous organic polymers based on tetraphenylanthraquinone for CO_2 uptake and high-performance supercapacitor

Mohamed Gamal Mohamed [a,b], Xian Zhang [c], Tharwat Hassan Mansoure [b], Ahmed F. M. EL-Mahdy [a,b], Chih-Feng Huang [d], Martin Danko [e], Zhong Xin [c], Shiao-Wei Kuo [a,f,*]

[a] Department of Materials and Optoelectronic Science, Center of Crystal Research, National Sun Yat-Sen University, Kaohsiung, 804, Taiwan
[b] Chemistry Department, Faculty of Science, Assiut University, Assiut, 71516, Egypt
[c] Shanghai Key Laboratory of Multiphase Materials Chemical Engineering, Department of Product Engineering, East China University of Science and Technology, Shanghai, 200237, People's Republic of China
[d] Department of Chemical Engineering, Research Center for Sustainable Energy and Nanotechnology, National Chung Hsing University, 145 Xingda Road, South District, Taichung, 40227, Taiwan
[e] Department of Synthesis and Characterization of Polymers, Polymer Institute, Slovak Academy of Sciences, Dúbravská cesta 9, Bratislava, 84541, Slovakia
[f] Department of Medicinal and Applied Chemistry, Kaohsiung Medical University, Kaohsiung, 807, Taiwan

ARTICLE INFO

Keywords:
Tetraphenylanthraquinone
Thermal stability
CO_2 uptake
Energy storage performance

ABSTRACT

We successfully synthesized two different kinds of hyper-crosslinked porous organic polymers (CPOPs) based on tetraphenylanthraquinone units by a reaction of 9,10-bis(diphenylmethylene)- 9,10-dihydroanthracene (An-4Ph) as the building unit with formaldehyde dimethyl acetal and 2,4,6-trichloro-1,3,5-triazine as two external crosslinkers by using a simple and friendly one-step Friedel–Crafts polymerization in the presence anhydrous $FeCl_3$ as a catalyst to afford An-CPOP-1 and An-CPOP-2 as a black solid with high yield, respectively. Fourier-transform infrared (FTIR) and NMR spectroscopy were confirmed the chemical structures of the synthesized monomers and the corresponding polymers. Both An-CPOP-1 and An-CPOP-2 showed amorphous character, outstanding thermal stability, and high BET surface area (up to 1000 m^2/g) with microporosity and mesoporosity architectures based on XRD, TGA analyses and N_2 adsorption/desorption measurements. Interestingly, TEM and SEM images revealed that An-CPOP-1 had regular tubular nanotubes structure without using template or surfactant or carbonization at the elevated temperature. The as-prepared An-CPOP-2 exhibited a high specific capacitance of 98.4 F g^{-1} at a current density of 0.5 A g^{-1} and excellent cycling stability (95.3% capacitance retention over 2000 cycles), which could be used as good material for energy storage application.

1. Introduction

Over the past decade, porous organic polymers (POPs) are type and emerging porous materials and have much attracted and attention in both academic and industry areas [1–4]. Because of their amazing properties such as low regeneration energy, synthetic diversity, large specific surface area, large pore volume, excellent thermal and chemical stability, facile functionalization, high porosity, diverse composition, and low density [5–9]. Due to their unique characters, POPs have been applied in many great potential applications such as biomedical, photovoltaics, energy storage, gas capture and separation, optical devices, photocatalysis, and sensors [10–18]. There are several categories from porous organic polymers, including porous aromatic frameworks (PAFs) [19], porous polymer networks (PPNs) [20], covalent triazine frameworks (CTFs) [21,22], covalent organic frameworks (COFs) [23–30], polymers of intrinsic microporosity (PIMs) [31], conjugated microporous polymers (CMPs) [32,33], hypercrosslinked porous polymers (HCPs) [34,35], and porous benzimidazole linked polymers (BILPs) [36,37]. As mentioned above, hypercrosslinked porous polymers (HCPs) are considered as a subclass of porous organic polymers (POPs) and remained important kinds of POPs because of their advantages including easy functionalization, judicious selection of monomers, high surface area, controlled reaction conditions, different synthetic categories, outstanding thermal stability, low-cost reagents, excellent chemical

* Corresponding author. Department of Materials and Optoelectronic Science, Center of Crystal Research, National Sun Yat-Sen University, Kaohsiung, Taiwan.
E-mail address: kuosw@faculty.nsysu.edu.tw (S.-W. Kuo).

https://doi.org/10.1016/j.polymer.2020.122857
Received 19 June 2020; Received in revised form 22 July 2020; Accepted 25 July 2020
Available online 30 July 2020
0032-3861/

robustness, and appropriate length crosslinkers to produce porous topology with a well-developed polymer framework [38–46]. There are three approaches to prepare HCPs: (i) one-step polycondensation of functional monomers; (ii) knitting rigid aromatic building blocks (such as benzene, anthracene, carbazole, naphthalene, and triphenylamine) with external crosslinkers and (iii) using post-crosslinking polymer precursors [38,43,47]. Therefore, by using these approaches to synthesize new HCPs with various pore architectures and high surface area to solve the environmental and energy issue [43]. Friedel–Crafts chemistry method is mainly used to prepare HCPs and this method provides a fast kinetic to form strong linkages and obtained a highly crosslinked network with adjusted porous topology [48–51]. As previously reported, the final skeleton construction of the final products of HCPs with the difference in the surface area and porosity can be controlled and adjusted by different rigidity and length of different linking units [40]. Davankov et al. prepared the first type of HCPs by post-crosslinking polystyrene through a Friedel–Crafts alkylation reaction and these materials displayed a high BET specific surface area up to 2090 $m^2\ g^{-1}$ [51]. Zou et al. prepared HCPs based on 9-phenylcarbazole (9-PCz) and these porous polymers exhibited narrow pore size distribution, high total pore volume, and BET specific surface areas were up to 769 $m^2\ g^{-1}$ [52]. Interestingly, Jiang et al. used different aromatic hydrocarbons (anthracene, pyrene, phenanthrene, and benzene) and their reaction with formaldehyde dimethyl acetal in the absence of any surfactant and template in the presence anhydrous $FeCl_3$ as a catalyst to afford a series of 1D hyper-crosslinked polymer nanotubes (HCPTs). Then, they used direct carbonization of these 1D tubular HCPTs to afford high-quality PCNTs with high surface area (921 $m^2\ g^{-1}$) [53]. These HCPs are interesting materials for supercapacitor applications and CO_2 storage due to its huge surface area, hierarchical porous structure; as well as facile and cost-effective preparation processes [16,34,40]. Regardless of the great progress in synthetic approaches, there are few reports on the supercapacitor performance of HCPs due to the lack of extended π-conjugated systems in HCP networks [54]. The supercapacitor performance of HCPs can be improved by two routes, the first route is based on using various building blocks for improving the surface area and pore-size distribution [5,43,45,53]. While, the second route relies on the heteroatoms doping (e.g. S, B, P, and N) in the carbon framework to enhance the electronic conductivity and electroactive surface area of the electrode [21–27]. In this regard, Wang et al. reported the synthesis of HCP nanotubes (HCPTs) using different aromatic building blocks (e.g., benzene, anthracene, phenanthrene, and pyrene) [53]. The benzene-based porous carbon nanotube (PCNT-B) showed a specific capacitance of 172 F g^{-1} at a current density of 0.5 A g^{-1}, which could remain 76.2% (131.4 F g^{-1}) at a high current density of 30 A g^{-1}. In addition, Lu et al. reported the synthesis of a series of N, S-doped hierarchically porous carbon (N, S-MC) derived by a hypercrosslinked polymerization approach [55]. The N, S-MC based electrode exhibited a specific capacitance of 464 F g^{-1} at 0.2 A g^{-1}, a high energy density of 16.2 W h kg^{-1} at 50 W kg^{-1} with capacitance retention of 92% after 10, 000 cycles. In this present study, we successfully prepared two different kinds of hypercrosslinked porous polymers based on tetraphenylanthraquinone units by the reaction of An-4Ph as building unit with formaldehyde dimethyl acetal and 2,4,6-trichloro-1,3,5-triazine as two different kinds of external crosslinker by using a simple one-step Friedel−Crafts polymerization in the presence $FeCl_3$ as a catalyst at 60 °C to afford An-CPOP-1 and An-CPOP-2 as a black solid with high yield. We carried out different measurements including FTIR and NMR spectroscopy to prove the chemical structures of the synthesized monomers and polymers. The thermal stability, crystallinity properties, morphology, and porosity of the synthesized HCPs based on tetraphenylanthraquinone units were investigated by X-ray diffraction (XRD), thermogravimetric analysis (TGA), transmission electron microscopy (TEM), scanning electron microscopy (SEM) and N_2 adsorption/desorption isotherm measurements. Finally, we performed electrochemical analyses to estimate their potential application as electrode materials for energy storage performance. It is the first report to study and present the electrochemical performance of hyper-crosslinked porous polymers based on tetraphenylanthraquinone units.

2. Experimental section

2.1. Materials

Anthracene-9,10-dione, carbon tetrabromide (CBr_4), triphenylphosphine (PPh_3), phenylboronic acid, tetrakis(triphenylphosphine)palladium ($Pd(PPh_3)_4$), anhydrous ferric chloride ($FeCl_3$), methanol (CH_3OH), tetrahydrofuran (THF), potassium carbonate (K_2CO_3), hydrochloric acid (HCl, 37%) and 2,4,6-trichloro-1,3,5-triazine were purchased from Sigma Aldrich. formaldehyde dimethyl acetal (FDA), tetrahydrofuran (THF), toluene, dichloromethane (DCM), 1,2-dichloroethane, and acetone were purchased from Acros.

2.2. Synthesis of 9,10-bis(dibromomethylene)-9,10-dihydroanthracene (An-4Br) [56]

In a 250 mL two neck-bottle flask, anthracene-9,10-dione (3.00 g, 14.41 mmol), carbon tetrabromide (23.90 g, 91.12 mmol) and triphenylphosphine (15.00 g, 45.23 mmol) was added. Then, the dry toluene (210 mL) was added into the flask and the mixture was cooled to −10 °C using ice bath and acetone. The reaction mixture was stirred for 1 h at −10 °C and then removed the ice bath and stirred at 80 °C for 24 h under N_2 atmosphere. After that, the insoluble material was removed by vacuum filtration. Then, the organic layer was evaporated by rotatory evaporator and recrystallization by methanol to afford a white solid. The solid powder was filtrated and dried under vacuum at 50 °C for 24 h to afford An-4Br (6.37 g, 85%). FTIR (KBr, cm^{-1}): 3067 (w, C–H), 1584 (m, aromatic C═C), 1562 (m, aromatic C═C), 1448, 1180, 1160, 1046, 934, 833, 765, 733, 637 and 615 cm^{-1}. ^1H NMR (500 MHz, $CDCl_3$), δ (ppm): 7.81–7.83 (m, 4H) and 7.26–7.28 (m, 4H). ^{13}C NMR (125 MHz, DMSO-d_6): δ (ppm) = 139.80, 135.95, 128.14, 91.44.

2.3. Synthesis of 9,10-bis(diphenylmethylene)-9,10-dihydroanthracene (An-4Ph)

In a 250 mL two neck-bottle flask, An-4Br (1.00 g, 1.92 mmol), phenylboronic acid (1.88 g, 15.42 mmol), tetrakis(triphenylphosphine) palladium ($Pd(PPh_3)_4$), (0.22 g, 0.19 mmol) and potassium carbonate (K_2CO_3, 2.13 g, 15.41 mmol) were dissolved in dry THF/H_2O (50/20 mL) and refluxed at 80 °C for 48 h. After that, the system was cooled to the room temperature and the insoluble material was removed by vacuum filtration. The organic layer was evaporated by the rotatory evaporator. Then, 200 mL H_2O and 2 mL HCl (37%) were poured into the mixture and the obtained solid powder was filtrated and washed using water. Finally, the crude product added into methanol companies with vigorous stirring for 1 h at room temperature and a white solid was filtrated to afford An-4Ph (1.12 g, 93%). FTIR (KBr, cm^{-1}): 3055 (aromatic C–H), 1597, 1571, 1486, 1440, 1284, 1070, 1028, 747, 705, 617, 591 cm^{-1}. ^1H NMR (500 MHz, DMSO-d_6), δ (ppm): 7.41 (d, $J = 8.20$ Hz, 8H), 7.28 (t, $J = 7.54$ Hz, 8H), 7.18 (t, $J = 7.54$ Hz, 4H), 6.98 (m, 4H) and 6.71 (m, 4H). ^{13}C NMR (500 MHz, DMSO-d_6), δ (ppm): 143.20, 140.54, 138.45, 136.28, 130.35, 128.86, 125.77, 125.5.

2.4. Synthesis of An-CPOP-1

In a 150 mL two neck-bottle flask, An-4Ph (0.60 g, 1.18 mmol), formaldehyde dimethyl acetal (0.62 mL, 7.00 mmol) and anhydrous $FeCl_3$ (1.14 g, 7.03 mmol) were added in 40 mL of dry 1.2-dichloroethane and the reaction mixture was refluxed for 24 h under N_2 atmosphere. The black solid was filtrated and washed using water, methanol, acetone, and THF to afford An-CPOP-1 (0.52 g, 80%). FTIR (cm^{-1}): 3430 (OH stretching), 3059 (CH aromatic), 2920, 2864 (CH aliphatic), 1601

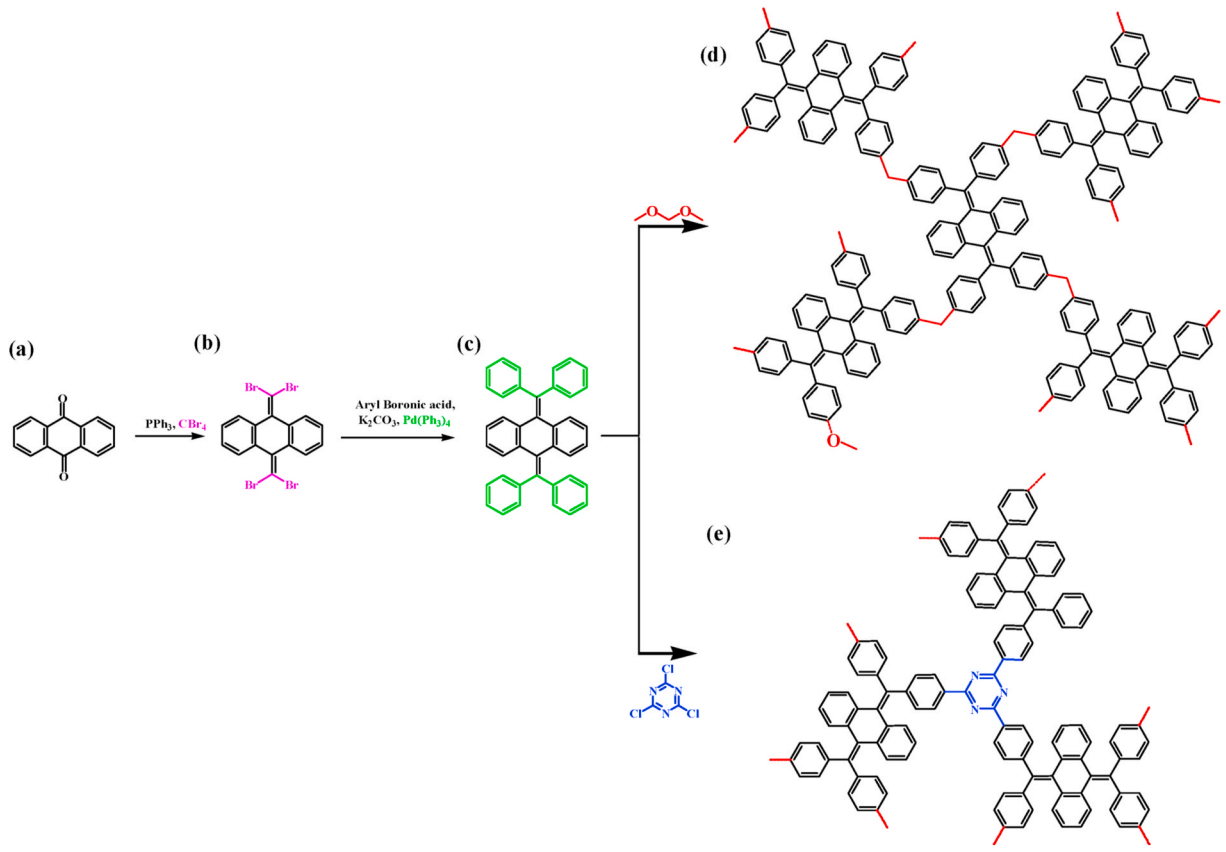

Scheme 1. Synthetic route to (d) An-CPOP-1 and (e) An-CPOP-2 via Friedel–Crafts alkylation polymerization reaction from (a) anthracene-9,10-dione, (b) An-4Br and (c) An-4Ph.

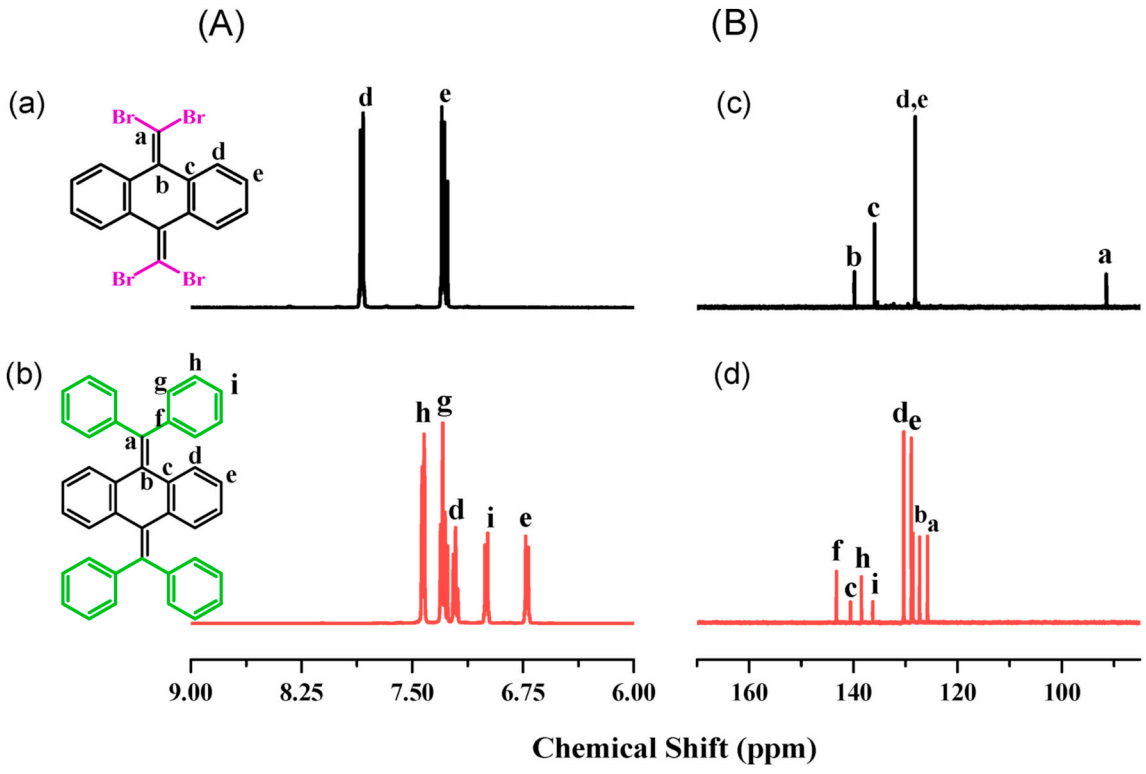

Fig. 1. (A) ^{1}H NMR spectra of (a) An-4Br and (b) An-4Ph. (B) ^{13}C NMR spectra of (c) An-4Br and (d) An-4Ph in DMSO-d_6.

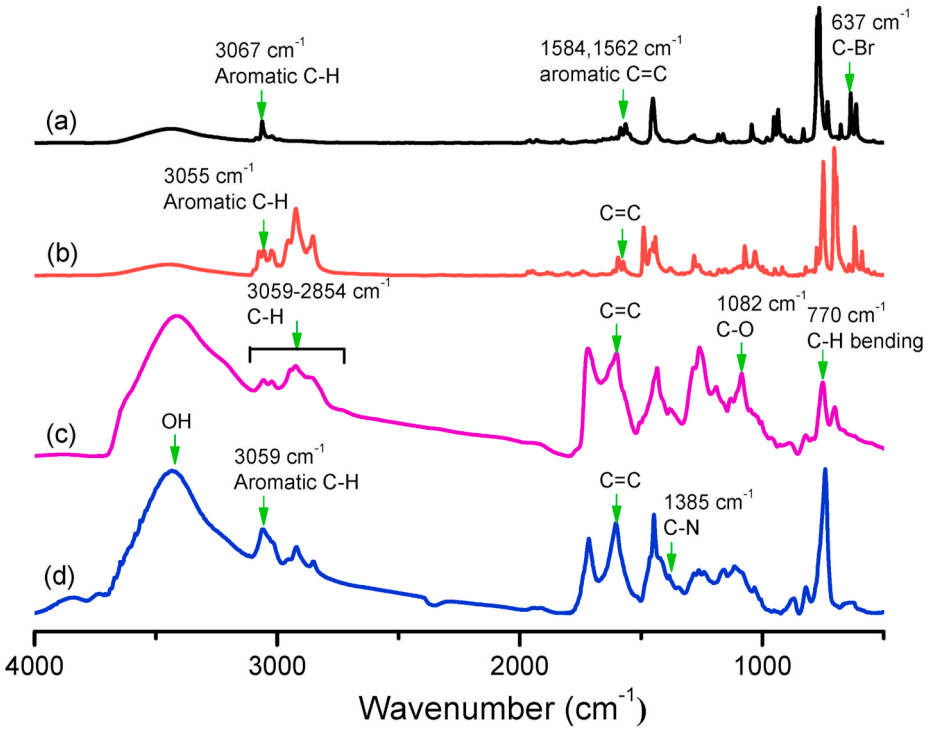

Fig. 2. FT-IR spectra of (a) An-4Br, (b) An-4Ph (c) An-CPOP-1 and (d) An-CPOP-2, recorded at room temperature.

(C═C), 1082 (C–O), 770 (CH bending).[13]C solid-state CP/MAS NMR (ppm, δ) = 114.31, 119.95, 102.25 (aromatic), 71.32 (CH_2).

2.5. Synthesis of An-CPOP-2

In a 150 mL two neck-bottle flask, An-4Ph (0.50 g, 0.98 mmol) and 2,4,6-trichloro-1,3,5-triazine (0.6 g, 3.25 mmol) and ferric chloride ($FeCl_3$, 0.77 g, 4.72 mmol) was added. Then, the flask was evacuated of the air under vacuum and filled with dry nitrogen three times. Then, dry 1.2-dichloroethane (30 mL) was added into the flask and the reaction refluxed for 24 h under a N_2 atmosphere. Then, the reaction mixture was cooled to room temperature and the solid powder was filtrated and washed with water, methanol, acetone, and THF. Finally, the crude product was added into methanol and vigorously stirred for 1 h at 70 °C.

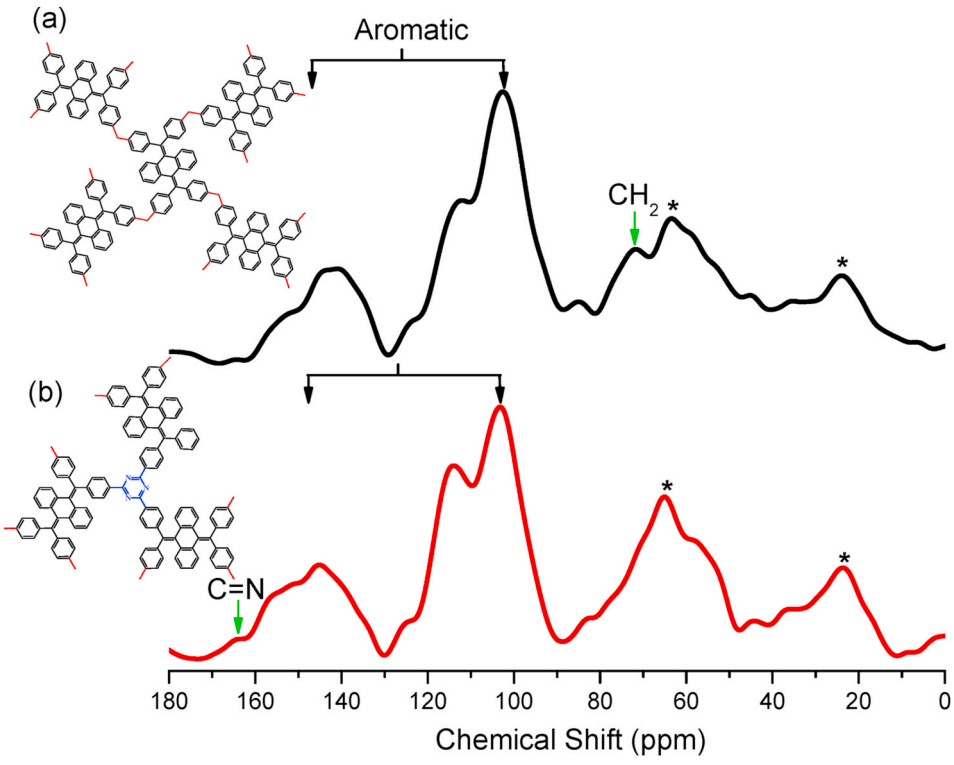

Fig. 3. [13]C CP/MAS NMR spectra of (a) An-CPOP-1 and (b) An-CPOP-2, recorded at room temperature. Asterisks denote spinning sidebands.

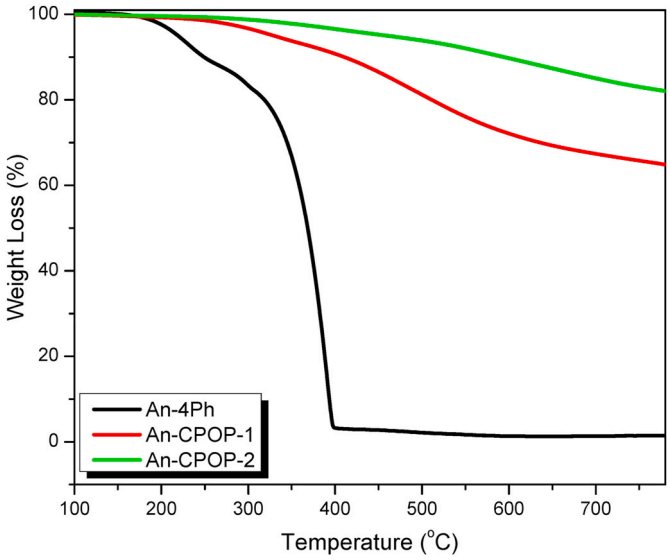

Fig. 4. Thermal stability of (a) An-4Ph, (b) An-CPOP-1, and (c) An-CPOP-2 by TGA analyses.

Then, the black solid was filtrated to afford An-CPOP-2 (0.51 g, 75%). FTIR (cm^{-1}): 3430 (OH stretching), 3059 (CH aromatic), 1601 (C═C), 1385 (C–N), 770 (CH bending). ^{13}C solid-state CP/MAS NMR (ppm, δ) = 163.96 (**C**═N), 145.29, 114.39, 102.78 (aromatic).

3. Results and discussion

3.1. Synthesis of An-CPOP-1 and An-CPOP-2

Scheme 1 summarizes the synthetic route of two kinds of tetraphenylanthraquinone-based porous organic polymers via the Friedel–Crafts alkylation reaction of An-4Ph with formaldehyde dimethyl acetal (FDA) and 2,4,6-trichloro-1,3,5-triazine as external crosslinking agents in the presence anhydrous $FeCl_3$ as a catalyst. First, anthracene-9,10-dione reacts with CBr_4 in the presence of triphenylphosphine (PPh_3) as a catalyst to afford An-4Br. Then, An-4Ph has obtained by a reaction of phenylboronic acid with An-4Br in THF/H_2O as co-solvent and $Pd(PPh_3)_4$ as a catalyst using Suzuki-Miyaura coupling reaction to afford An-4Ph as a white solid with high yield and purity.

The chemical structures of An-4Br and An-4Ph were confirmed by spectroscopic analyses (NMR and FTIR). Fig. 1 displays ^{1}H and ^{13}C NMR spectra of An-4Br and An-4Ph in DMSO-d_6 as a solvent. The characteristic proton signals of An-4Br (Fig. 1(A)(a)) appeared at 7.83 and 7.28 ppm corresponding to aromatic protons. The ^{1}H NMR spectrum of the An-4Ph features signals at 7.42, 7.29, 7.21, 6.99, and 6.73 ppm for the aromatic protons, as shown in the (Fig. 1(A)(b)). The ^{13}C NMR spectrum of An-4Br (Fig. 1(B)(c)) reveals signals at 139.80, 135.95, 128.14, and 91.44 ppm for its aromatic carbon nuclei. While, The ^{13}C NMR spectrum of An-4Ph (Fig. 1(B)(d)) features signals at 143.22, 138.46, 130.35, and 128.87 ppm for the aromatic nuclei and 127.29 and 125.76 ppm for the C═C carbon nuclei, respectively.

The FTIR spectrum of An-4Br (Fig. 2(a)) shows the absorptions bands at 3067 cm^{-1} for the stretching C–H aromatic, 1584, 1562 cm^{-1} for C═C stretching and 637 cm^{-1} for C–Br stretching. The absorption signal for C–Br stretching disappeared and characteristic absorptions for An-4Ph (Fig. 2(b)) appeared at 3055 cm^{-1} for aromatic C–H units, indicating the successful synthesis of An-4Ph. The absorption bands for the An-CPOP-1 (Fig. 2(c)) appear at 3059 cm^{-1} for aromatic C–H stretching

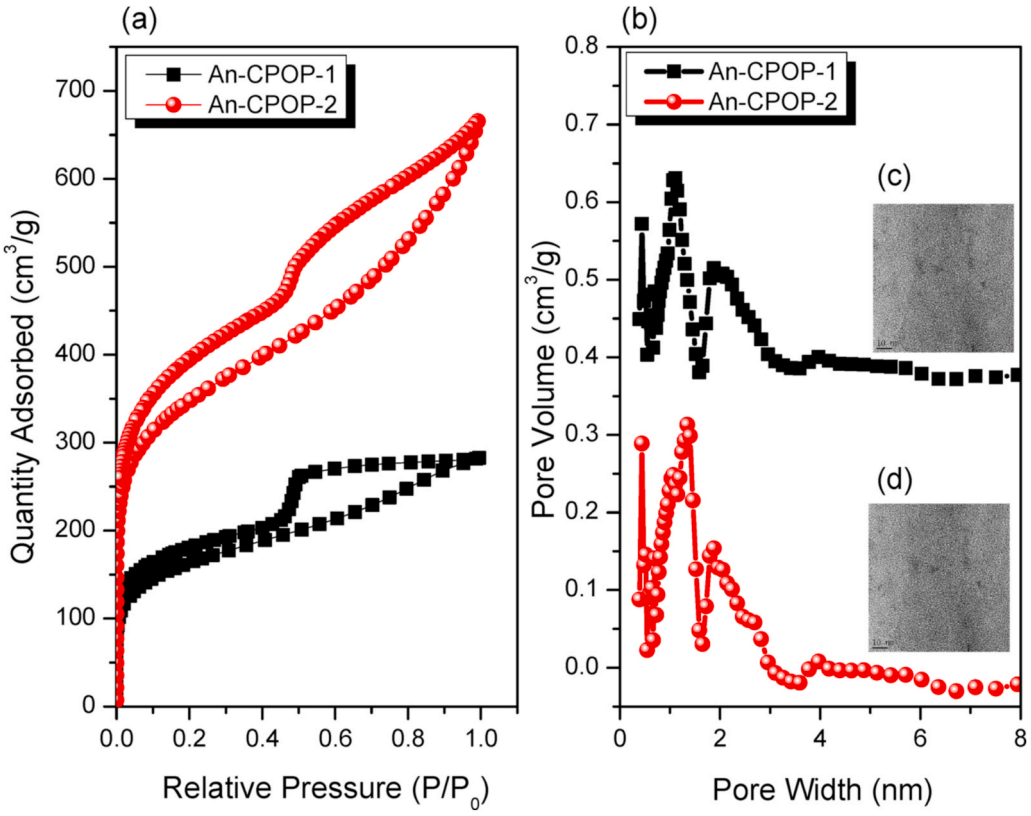

Fig. 5. (a) N_2 adsorption/desorption isotherms and (b) of pore size distribution curves calculated by NL-DFT method of An-CPOP-1 and An-CPOP-2, recorded at 77 K. Inset, TEM images of (c) An-CPOP-1 and (d) An-CPOP-2, respectively.

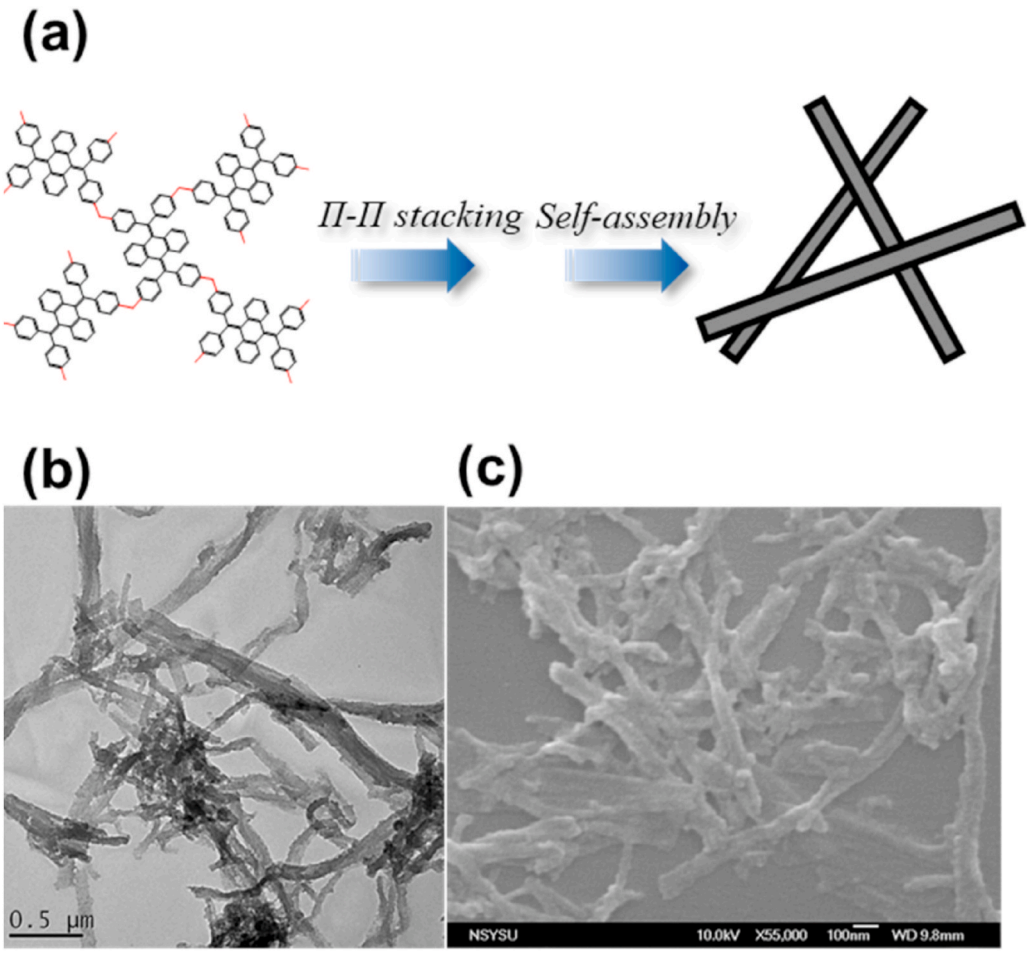

Fig. 6. (a) The proposed mechanism of tubular structure formation of An-CPOP-1, (b) TEM, and (c) SEM image of An-CPOP-1.

vibrations and 2920 and 2864 cm^{-1} which is assigned to the aliphatic C–H for CH_2 units and 1082 cm^{-1} for C–O stretching vibration (O–CH_3 units) in An-CPOP-1 [54]. The spectrum of An-CPOP-2 (Fig. 2(d)) features characteristic absorptions bands at 1715 cm^{-1} for C═N stretching and 1385 cm^{-1} for (C–N), indicating the presence of a triazine unit in the An-CPOP-2 network [57–59]. The overlapping and broader peak from 3100 to 3700 cm^{-1} was attributed to the stretching vibrations of the adsorbed H_2O by porous An-CPOP-1 and An-CPOP-2 materials.

To further confirm the successful synthesis of An-CPOP-1 and An-CPOP-2, we carried out the solid-state ^{13}C CP/MAS NMR measurements (Fig. 3). The solid-state ^{13}C NMR spectrum of the An-CPOP-1 (Fig. 3(a)) features signals at 141.31, 119.95, 102.25, and 71.32 ppm for its substituted phenyl carbons bonding to other aromatic rings, unsubstituted phenyl carbons and CH_2 carbon nuclei, respectively [60]. In Fig. 3(b), the characteristic signals for An-CPOP-2 appeared at 163.96, 145.39, 114.01, and 102.78 ppm for the carbon atoms in the triazine unit, and the aromatic carbon nuclei, respectively. Overall, the FTIR and NMR spectral data confirmed the successful incorporation of dimethoxymethane and 2,4,6-trichloro-1,3,5-triazine as external cross-linking agents and synthesis of tetraphenyl anthraquinone-based porous organic polymers [An-CPOP-1 and An-CPOP-2] with good yield.

Thermal stability of An-4Ph, An-CPOP-1, and An-CPOP-2 was examined by using thermogravimetric analysis (TGA) under an N_2 atmosphere, as presented in Fig. 4 and Table S1. We used T_{d5} (5% weight-loss temperature), T_{d10} (10% weight-loss temperature), and char yield to investigate thermal stability for these materials. An-4Ph exhibited degradation temperatures of 219 and 247 °C, respectively, and a char yield of 1.4 wt%. While, An-CPOP-1 and An-CPOP-2 showed high decomposition temperatures at 329, 410 °C, and 460, 595 °C, respectively. Furthermore, the polymer residue of An-CPOP-1 and An-CPOP-2 was 65 and 82 wt%, respectively, at 800 °C. It is worth mentioning that An-CPOP-2 showed excellent thermal stability compared to An-CPOP-1 and An-4Ph which is attributed to the presence of triazine units and its rigid fused aromatic structure. Overall, An-CPOP-1 and An-CPOP-2 displayed outstanding thermal stability compared to other porous organic polymers [60].

The textural properties including porosity and BET specific surface area of An-CPOP-1 and An-CPOP-2 were determined by using N_2 adsorption and desorption measurements at 1 bar, as presented in Fig. 5 (a). Based on the IUPAC classification, The BET isotherms profile of An-CPOP-1 and An-CPOP-2 exhibited type I and type IV and increase N_2 uptake at low pressure which presenting the presence microporous structure of these materials. Also, there is a hysteresis loop at a relatively high-pressure region demonstrating the existence of mesoporosity nature for An-CPOP-1 and An-CPOP-2. Fig. 5(b) displays the pore size distribution curves of An-CPOP-1 and An-CPOP-2 which obtained by using nonlocal density functional theory (NLDFT), respectively. The obtained results reveal that An-CPOP-1 possess pore size diameters in the range of 0.38–1.91 nm. While the width of the pores for An-CPOP-2 was appeared at 0.48, 1.05, 1.35, 1.93, 2.74, and 4.01, respectively. Finally, the Brunauer– Emmett–Teller (BET) surface areas for An-CPOP-1 and An-CPOP-2 were 580 and 1130 $m^2\ g^{-1}$ with total pore volumes of 0.44 and 1.02 $cm^3\ g^{-1}$, respectively. We found that the specific surface area for An-CPOP-2 (1130 $m^2\ g^{-1}$) is lower than that of the other reported organic porous polymers such as the tetraphenylethylene-based HCPs (1980 $m^2\ g^{-1}$), porous organic frameworks based on carbazole (2065 $m^2\ g^{-1}$), tetraphenylmethane-based HCPs (1679 $m^2\ g^{-1}$), and higher than that the HCPs based on

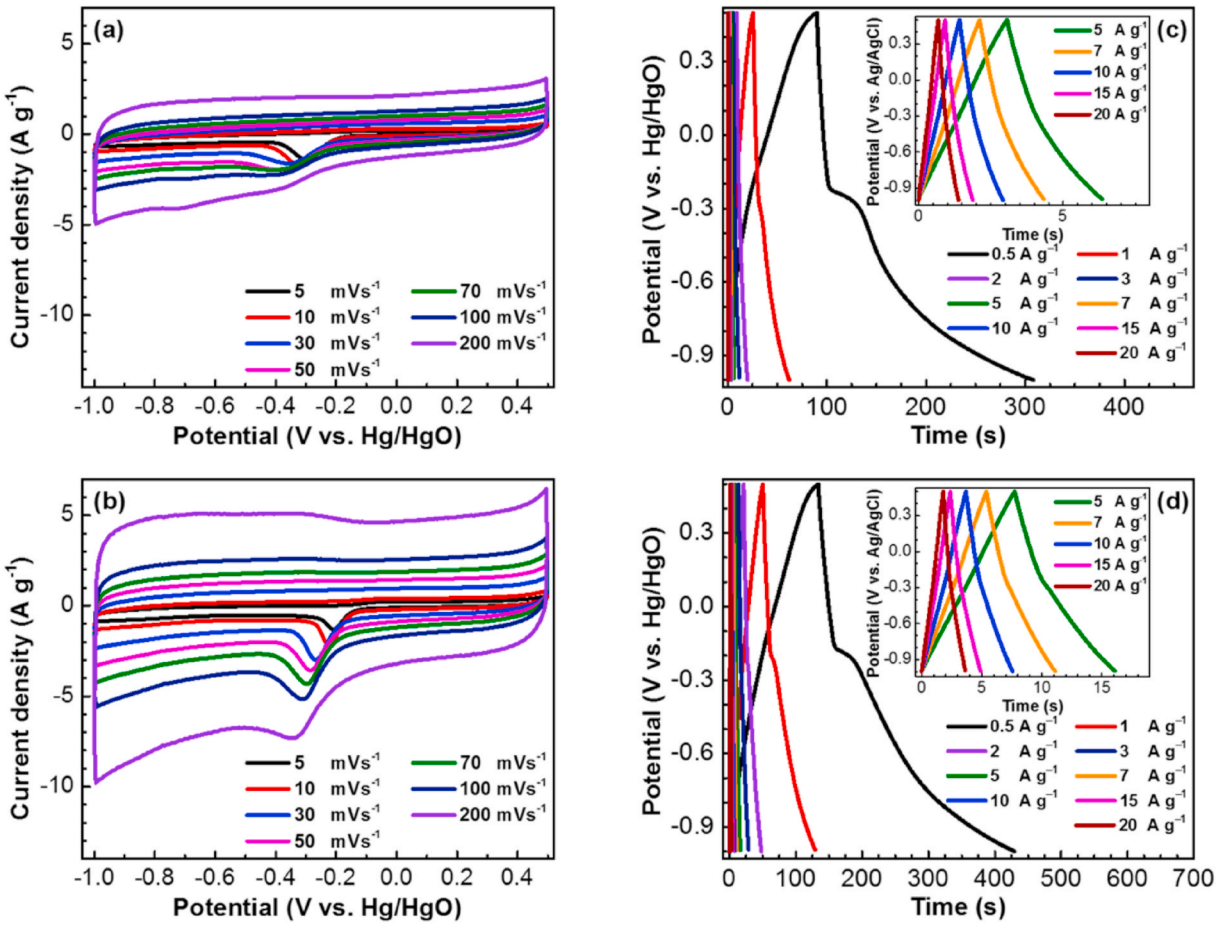

Fig. 7. (a, b) CV and (c, d) GCD profiles, recorded in 1 M KOH, of the (a, c) An-CPOP-1, and (b, d) An-CPOP-2.

binaphthol (1015 $m^2 g^{-1}$), porous organic polymer TSP-2 functionalized with triazine and carbazole units (913 $m^2 g^{-1}$) and HCP networks [5, 61–64] which might to the presence hierarchical porous structure and abundant mesoporous and microporous in the An-CPOP-2 networks.

TEM images (Fig. 5(c) and (d)) of An-CPOP-1 and An-CPOP-2 displayed these materials contain pores structure. the powder-X-ray-diffraction profile (Fig. S1) displayed the abroad diffractions peaks at 13°, 19°, and 41.70° for An-CPOP-1 and An-CPOP-2 showed three broad diffractions peaks at 12.70°, 20.17° and 43°, which indicating that An-CPOP-1 and An-CPOP-2 had amorphous nature. The morphology and microstructure of An-CPOP-1 and An-CPOP-2 were examined by transmission electron microscopy (TEM) and scanning electron microscopy (SEM). The morphology of An-CPOP-1 (Fig. 6(b) and (c)) showed nanotubes structures and the tubular surface was smoother. We attempt to explain the specific nanotube-like morphology for An-CPOP-1 [seen by SEM and TEM], as displayed in Fig. 6(a-c). Some studies revealed that anisotropic shape morphology originated from the geometries different during the formation of polymer network structures. Also, they discovered the solvents and geometries which are used for polymerizations have a strong effect on the morphology structure for the obtained polymers [60,65,66]. As shown in Fig. 6(a), the chemical structure of An-CPOP-1 contains a flexible cross-linkers and its flat geometry. Thus, the network of polymer chains of An-CPOP-1 has the freedom to move which leads to forming regular tubular structures. Furthermore, these flexible cross-linkers connected to tetraphenylanthraquinone units which undergo to form a 1D connection, and then interconnection of 1D chains. In contrast, the polymer chains of An-CPOP-2 possess were more rigid cross-linkers and leading to restrict the moving polymer chains and finally obtained agglomerated spherical morphology as displayed in SEM image (Fig. S2).

CO_2 uptake performance (Fig. S3 and Table S2) of the An-CPOP-1 and An-CPOP-2 was investigated using CO_2 isotherms measurements at 298 and 273 K, respectively. AT 273 K, both An-CPOP-1 and An-CPOP-2 show CO_2 capture of 1.40 and 1.52 mmol/g, respectively. At 298 K and 1 bar, the CO_2 uptake for An-CPOP-1 and An-CPOP-2 was 1.30 and 1.40 mmol/g, as observed in Fig. S3(a), An-CPOP-2 showed excellent CO_2 uptake value (1.52 mmol/g) than that An-CPOP-1 (1.40 mmol/g) probably due to its high BET surface area, large pore size and existence the triazine units in An-CPOP-2, which could also lead to good interaction and binding affinity between CO_2 molecules and N atoms in triazine rings. Our materials feature lower value of CO_2 uptake capacity compared with other HCPs materials under the same temperatures, for example, hypercrosslinked porous polymers (HCPs) based on tetraphenylethylene (3.63 mmol/g), triphenylbenzene (3.61 mmol/g), tetraphenylmethane (2.27 mmol/g), binaphthol-based BINOL (3.96 mmol/g), porous organic frameworks based on carbazole (4.77 mmol/g), PPF-1 (6.1 mmol/g), polythiophene-based Th-1 (2.89 mmol/g), and porous functionalized TSP-2 with triazine units (4.1 mmol/g) [5,60–64]. Interestingly, our materials still exhibited higher CO_2 uptake than that of the silole based HCPs (e.g. 1.02 mmol/g for PDMTPAS and 1.04 mmol/g for PDPTPAS at 298 K) and 1.44 mmol/g for C2M1-Al at 273 K) [67,68] which could be attributed to the higher BET surface area, pore-volume, and strong dipole–quadrupole interactions between the An-CPOPs materials with the CO_2 molecules.

3.2. Electrochemical results

Cyclic voltammetry (CV) and galvanostatic charge-discharge (GCD) have been used to examine the electrochemical performances of our An-based CPOPs in a three-electrode system with 1 M KOH as the aqueous

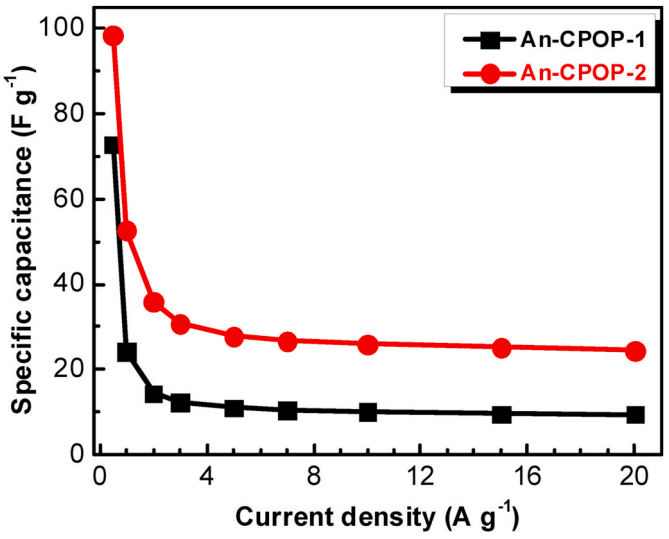

Fig. 8. Corresponding specific capacitances of An-CPOP-1 and An-CPOP-2 determined at various current densities.

electrolyte. Fig. 7a and b display the corresponding CV curves of An-CPOP-1 and An-CPOP-2, respectively, recorded at various sweep rates from 5 to 200 mV s^{-1} in the potential window from +0.50 to −1.00 V (vs. Hg/HgO). The An-CPOP-2 provided a relatively higher current density compared to that of An-CPOP-1. The corresponding CV curves of these two CPOPs samples had rectangle-like shapes featuring humps, indicating that this capacitive response originated from electric double-layer capacitance (EDLC) [25,53,69,70]. The distinct appearance of humps in the rectangle-like shape is an indication of pseudocapacitance arising from the presence of the electroactive methylene groups, and the nitrogen heteroatoms in the case of An-CPOP-2 [25,27,55]. Moreover, the current density increased upon increasing the sweep rate, while the shape of the CV curve was retained (Fig. 7a and b), indicating a good rate capability and facile kinetics. Fig. 7c and d present the GCD curves of the An-CPOP-1 and An-CPOP-2, respectively, measured at various current densities from 0.5 to 20 A g^{-1}. These GCD curves had triangular shapes featuring a slight bend, suggesting both pseudocapacity and EDLC characteristics [20,22] The discharging time of the An-CPOP-2 was longer than that of the An-CPOP-1 (Fig. 7c and d), indicating that the capacitance of the former was larger than that of the latter.

We used equation (**S1**) to determine the specific capacitances from the GCD curves (Fig. 8). The specific capacitance of the An-CPOP-2 (98.40 F g^{-1}) was larger than that of the An-CPOP-1 (72.75 F g^{-1}) at a current density of 0.5 A g^{-1}. This excellent performance of the An-CPOP-2 was due to its higher surface area (1130 m^2 g^{-1}) and pore volume (1.02 cm^3 g^{-1}), along with its heteroatoms, all of which made it easier for the electrolytes to access the surface of the electrode [71]. Peng et al. reported hollow ordered mesoporous carbon nanospheres (HOMCNSs) having a capacitance of 72.79 F g^{-1} at 0.5 A g^{-1} [72]. In addition, Liu et al. reported TpPa–COF/PANI composited exhibiting a capacitance of 95 F g^{-1} at 0.2 A g^{-1} [73]. Moreover, DAAQ–TFP COF showed capacitance of approximately 48 F g^{-1}at 0.1 A g^{-1} that did not decrease significantly after 5000 cycles [74]. Recently, our group reported the Car-TPA, Car-TPP, and Car-TPT COFs with capacitances of 13.6, 14.5, and 17.4 F g^{-1}, respectively, at 0.2 A g^{-1} [75]; as well as the TPA–COF–1, TPA–COF–2, TPA–COF–3, TPT–COF–4, TPT–COF–5, and TPTCOF-6 with capacitances of 51.3, 14.4, 5.1, 2.4, 0.34, and 0.24 F g^{-1}, respectively, at 0.2 A g^{-1} [28]. Furthermore, Khattak et al. reported a DAB–TFP COF having a capacitance of 98 F g^{-1} at 0.5 A g^{-1} [76]. Lyu and his workers reported that the tetraphenylporphyrin based polymer (HCTPP) possesses a specific capacitance of 179 F g^{-1} [54]. Also, Thomas et al. reported that 3D polyaminoanthraquinone (PAQ) networks displayed a specific capacitance of 576 F g^{-1} at 1 A g^{-1} in 0.5 M H_2SO_4 [77]. Pang et al. prepared two kinds of conjugated microporous polymers, TAT-CMP-1 and TAT-CMP-2 based on triazatruxene units, and these materials showed specific capacitance of 141 F g^{-1} for TAT-CMP-1 and 183 F g^{-1} for TAT-CMP-2 [78].

Table S3 summarizes the corresponding surface areas and specific capacitances. We examined the durability of our Anthra-based POPs by cycling them over 2000 times at 10 A g^{-1} (Fig. 9a and b). These two An-CPOP-1 and An-CPOP-2 displayed excellent cycling stability, with 98.7 and 95.3% retention, respectively, of their original capacitances after 2000 cycles. The related Ragone plot (Fig. S4) suggested that these two An-based CPOPs electrodes possessed good energy and power densities.

4. Conclusions

To conclude, we successfully prepared two kinds of CPOPs based on the tetraphenylanthraquinone units with good yield through one-step Friedel−Crafts polymerization based on FTIR and NMR spectroscopy. The as-prepared An-CPOP-2 through the reaction with 2,4,6-trichloro-1,3,5-triazine exhibited significant supercapacitor performance (up to 98.4 F g^{-1} at a current density of 0.5 A g^{-1}), excellent cycling stability (95.3% capacitance retention over 2000 cycles), and a high energy density (30.75 Wh kg^{-1}). This excellent performance of the An-CPOP-2 could be attributed to its higher surface area along with the presence of the nitrogen heteroatoms (triazine units) which made it easier for the

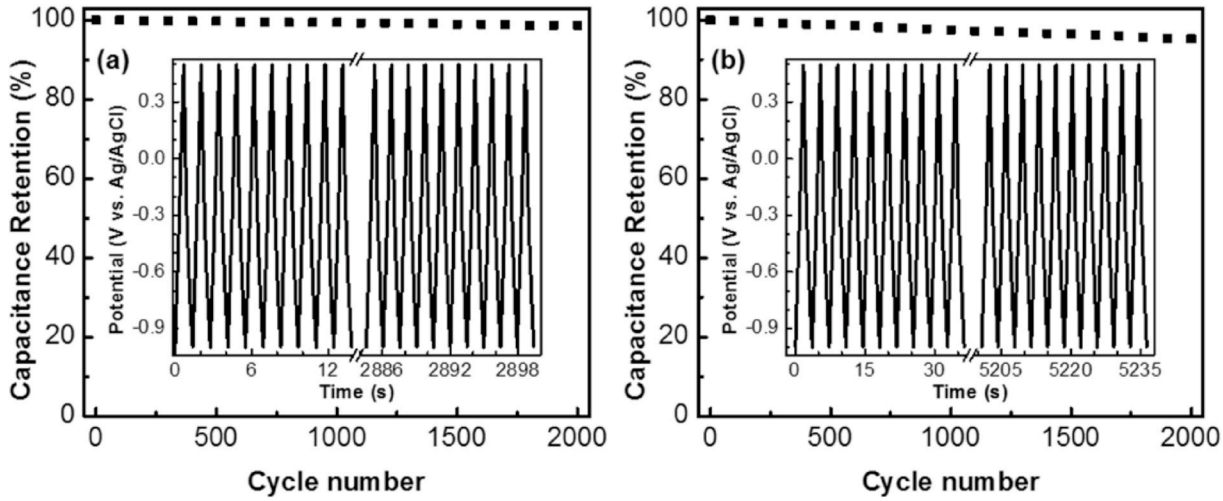

Fig. 9. Cycling performance of (a) An-CPOP-1 and (b) An-CPOP-2 measured at a current density of 10 A g^{-1} for 2000 cycles.

electrolytes to access the surface of the electrode.

CRediT authorship contribution statement

Mohamed Gamal Mohamed: Methodology, Investigation, Formal analysis, Writing - original draft, Writing - review & editing. **Xian Zhang:** Investigation. **Tharwat Hassan Mansoure:** Investigation. **Ahmed F.M. EL-Mahdy:** Investigation. **Chih-Feng Huang:** Supervision. **Martin Danko:** Supervision. **Zhong Xin:** Supervision. **Shiao-Wei Kuo:** Supervision, Writing - original draft, Writing - review & editing.

Declaration of competing interest

The authors declare that they have no known competing financial interests or personal relationships that could have appeared to influence the work reported in this paper.

Acknowledgements

This study was supported financially by the Ministry of Science and Technology, Taiwan, under contracts MOST 108-2638-E-002-003-MY2, 106-2221-E-110-067-MY3, 108-2221-E-110-014-MY3, and 108-2218-E-110-013-MY3. This work was also supported by the National Natural Science Foundation of China (51773214) and by SAS-MOST Joint Research Project "Tough-VigNet SAS-MOST JRP 2019/07. We also thank Mr. Hsien-Tsan Lin of the Regional Instruments Center at National Sun Yat-Sen University for help with the TEM measurement.

Appendix A. Supplementary data

Supplementary data related to this article can be found at https://doi.org/10.1016/j.polymer.2020.122857.

References

[1] Y. Byun, S.H. Je, S.N. Talapanani, A. Coskun, Advances in porous organic polymers for efficient water capture, Chem. Eur J. 25 (2019) 10262–10283.
[2] T.X. Wang, H.P. Liang, D.A. Anito, X. Ding, B.H. Han, Emerging applications of porous organic polymers in visible-light photocatalysis, J. Mater. Chem. A 8 (2020) 7003–7034.
[3] W.C. Chen, M.M.M. Ahmed, C.F. Wang, C.F. Huang, S.W. Kuo, Highly thermally stable mesoporous Poly(cyanate ester) featuring double-decker–shaped polyhedral silsesquioxane framework, Polymer 185 (2019) 121940–121950.
[4] K.I. Aly, M.M. Sayed, M.G. Mohamed, S.W. Kuo, O. Younis, A facile synthetic route and dual function of network luminescent porous polyester and copolyester containing porphyrin moiety for metal ions sensor and dyes adsorption, Micropor. Mesopor. Mater. 298 (2020), 110063.
[5] X. Yang, M. Yu, Y. Zhao, C. Zhang, X. Wang, J.X. Jiang, Hypercrosslinked microporous polymers based on carbazole for gas storage and separation, RSC Adv. 4 (2014) 61051–61055.
[6] S. Das, P. Heasman, T. Ben, S. Qiu, Porous organic materials: strategic design and structure−function correlation, Chem. Rev. 117 (2016) 1515–1563.
[7] R. Dawson, A.I. Cooper, D.J. Admas, Chemical functionalization strategies for carbon dioxide capture in microporous organic polymers, Polym. Int. 62 (2013) 345–352.
[8] H. Furukawa, O.M. Yaghi, Storage of hydrogen, methane, and carbon dioxide in highly porous covalent organic frameworks for clean energy applications, J. Am. Chem. Soc. 131 (2009) 8875–8883.
[9] H.R. Abuzeid, A.F.M. EL-Mahdy, M.M.M. Ahmed, S.W. Kuo, Triazine-functionalized covalent benzoxazine framework for direct synthesis of N-doped microporous carbon, Polym. Chem. 10 (2019) 6010–6020.
[10] Y. Cui, J. Du, Y. Liu, Y. Yu, S. Wang, H. Pang, Z. Liang, J. Yu, Design and synthesis of multifunctional porous N-rich polymer containing s-triazine and Tröger's base for CO_2 adsorption, catalysis and sensing, Polym. Chem. 9 (2018) 2643–2649.
[11] N.B. McKeown, P.M. Budd, D. Book, Microporous polymers as potential hydrogen storage materials, Macromol. Rapid Commun. 28 (2007) 995–1002.
[12] X. Zou, H. Ren, G. Zhu, Topology-directed design of porous organic frameworks and their advanced applications, Chem. Commun. 49 (2013) 3925–3936.
[13] T. Ma, X. Zhao, Y. Matsuo, J. Song, R. Zhao, M. Faheem, M. Chen, Y. Zhang, Y. Tian, G. Zhu, Fluorescein-based fluorescent porous aromatic framework for Fe^{3+} detection with high sensitivity, J. Mater. Chem. C. 7 (2019) 2327–2332.
[14] H. Lv, W. Wang, F. Li, Porous organic polymers with built-in N-heterocyclic carbenes: selective and efficient heterogeneous catalyst for the reductive N-formylation of amines with CO_2, Chem. Eur J. 24 (2018) 16588–16594.
[15] M.G. Mohamed, S.M. Ebrahium, A.S. Hammam, S.W. Kuo, K.I. Aly, Enhanced CO_2 capture in nitrogen-enriched microporous carbons derived from Polybenzoxazines containing azobenzene and carboxylic acid units, J. Polym. Res. 27 (2020) 197.
[16] M.G. Mohamed, W.S. Hung, A.F.M. EL-Mahdy, M.M.M. Ahmed, L. Dai, T. Chen, S. W. Kuo, High-Molecular-weight PLA-b-PEO-b-PLA triblock copolymer templated large mesoporous carbons for supercapacitors and CO_2 capture, Polymers 12 (2020) 1193.
[17] R. Kumar, R. Shunmugam, Unique design of porous organic framework Showing efficiency toward removal of toxicants, ACS Omega 2 (2017) 4100–4107.
[18] W.T. Li, Y.T. Zhuang, J.Y. Wang, T. Yang, Y.L. Yu, M.L. Chen, J.H. Wang, A three-dimensional porous organic framework for highly selective capture of mercury and copper ions, ACS Appl. Polym. Mater. 1 (2019) 2797–2806.
[19] T. Ben, H. Ren, S. Ma, D. Cao, J. Lan, X. Jing, W. Wang, J. Xu, F. Deng, J. M. Simmons, S. Qiu, G. Zhu, Targeted synthesis of a porous aromatic framework with high stability and exceptionally high surface area, Angew. Chem. Int. Ed. 48 (2009) 9457–9460.
[20] D. Yuan, W. Lu, D. Zhao, H.C. Zhou, Highly stable porous polymer networks with exceptionally high gas-uptake capacities, Adv. Mater. 23 (2011) 3723–3725.
[21] M. Liu, L. Guo, S. Jin, B. Tan, Covalent triazine frameworks: synthesis and applications, J. Mater. Chem. A 7 (2019) 5153–5172.
[22] M.G. Mohamed, A.F.M. EL-Mahdy, M.M.M. Ahmed, S.W. Kuo, Direct synthesis of microporous bicarbazole-based covalent triazine frameworks for high-performance energy storage and carbon dioxide uptake, ChemPlusChem 84 (2019) 1767–1774.
[23] M.G. Mohamed, C.C. Lee, A.F.M. EL-Mahdy, J. Luder, M.H. Yu, Z. Li, Z. Zhu, C. C. Chueh, S.W. Kuo, Exploitation of two-dimensional conjugated covalent organic frameworks based on tetraphenylethylene with bicarbazole and pyrene units and applications in perovskite solar cells, J. Mater. Chem. A 8 (2020) 11448–11459.
[24] M.G. Mohamed, A.F.M. EL-Mahdy, Y. Takashi, S.W. Kuo, Ultrastable conductive microporous covalent triazine frameworks based on pyrene moieties provide high-performance CO_2 uptake and supercapacitance, New J. Chem. 44 (2020) 8241–8253.
[25] A.F.M. EL-Mahdy, M.G. Mohamed, T.H. Mansoure, H.H. Yu, T. Chen, S.W. Kuo, Ultrastable tetraphenyl-p-phenylenediamine-based covalent organic frameworks as platforms for high-performance electrochemical supercapacitors, Chem. Commun. 55 (2019) 14890–14893.
[26] T. Li, X. Yan, Y. Liu, W.D. Zhang, Q.T. Fu, H. Zhu, Z. Li, Z.G. Gu, A 2D covalent organic framework involving strong intramolecular hydrogen bonds for advanced supercapacitors, A 2D covalent organic framework involving strong intramolecular hydrogen bonds for advanced supercapacitors, Polym. Chem. 11 (2020) 47–52.
[27] A.P. Côté, A.I. Benin, N.W. Ockwig, M. O'Keeffe, A.J. Matzger, O.M. Yaghi, Porous, crystalline, covalent organic frameworks, Science 310 (2005) 1166–1170.
[28] A.F.M. EL-Mahdy, C.H. Kuo, A. Alshehri, C. Young, Y. Yamauchi, J. Kim, S.W. Kuo, Strategic design of triphenylamine- and triphenyltriazine-based two-dimensional covalent organic frameworks for CO_2 uptake and energy storage, J. Mater. Chem. A 6 (2018) 19532–19541.
[29] A.F.M. EL-Mahdy, Y.H. Hung, T.H. Mansoure, H.H. Yu, Y.S. Hsu, K.C.W. Wu, S. W. Kuo, Synthesis of [3+ 3] β-ketoenamine-tethered covalent organic frameworks (COFs) for high-performance supercapacitance and CO_2 storage, J. Taiwan Inst. Chem. Eng. 103 (2019) 199–208.
[30] H.R. Abuzeid, A.F.M. EL-Mahdy, S.W. Kuo, Hydrogen bonding induces dual porous types with microporous and mesoporous covalent organic frameworks based on bicarbazole units, Micropor. Mesopor. Mater. 300 (2020), 110151.
[31] O. Vopička, K. Friess, V. Hynek, P. Sysel, M. Zgazar, M. Sipek, M.K. Pilnacek, M. Lanc, J.C. Jansen, C.R. Mason, P.M. Budd, Equilibrium and transient sorption of vapours and gases in the polymer of intrinsic microporosity PIM-1, J. Membr. Sci. 434 (2013) 148–160.
[32] S. Wang, Y. Liu, Y. Ye, X. Meng, J. Du, X. Song, Z. Liang, Ultrahigh volatile iodine capture by conjugated microporous polymer based on N,N,N',N'-tetraphenyl-1,4-phenylenediamine, Polym. Chem. 10 (2019) 2608–2615.
[33] J.X. Jiang, F. Su, A. Trewin, C.D. Wood, N.L. Campbell, H. Niu, C. Dickinson, A. Y. Ganin, M.J. Rosseinsky, Y.Z. Khimyak, A.I. Cooper, Conjugated microporous poly(aryleneethynylene) networks, Angew. Chem. Int. Ed. 46 (2007) 8574.
[34] L. Pan, Q. Chen, J.H. Zhu, J.G. Yu, Y.J. He, B.H. Han, Hypercrosslinked porous polycarbazoles via one-step oxidative coupling reaction and Friedel–Crafts alkylation, Polym. Chem. 6 (2015) 2478–2487.
[35] J. Germain, J. Hradil, J.M.J. Frechet, F. Svec, High surface area nanoporous polymers for reversible hydrogen storage, Chem. Mater. 18 (2006) 4430–4435.
[36] M.G. Rabbani, H.M. El-Kaderi, Synthesis and characterization of porous benzimidazole-linked polymers and their performance in small gas storage and selective uptake, Chem. Mater. 24 (2012) 1511–1517.
[37] H. Yu, M. Tian, C. Shen, Z. Wang, Facile preparation of porous polybenzimidazole networks and adsorption behavior of CO_2 gas, organic and water vapors, Polym. Chem. 4 (2013) 961–968.
[38] M.P. Tsyurupa, V.A. Davankov, Porous structure of hypercrosslinked polystyrene: state-of-the-art mini review, React. Funct. Polym. 66 (2006) 768–779.
[39] N. Fontanals, R.M. Marce, F. Borrull, P.A.G. Cormack, Hypercrosslinked materials: preparation, characterisation, and applications, Polym. Chem. 6 (2015) 7231–7244.
[40] L. Tan, B. Tan, Hypercrosslinked porous polymer materials: design, synthesis, and applications, Chem. Soc. Rev. 46 (2017) 3322–3356.
[41] V.A. Davankov, M.P. Hypercrosslinked, Polymeric Networks and Adsorbing Materials: Synthesis, Properties, Structure, and Applications, 56, Elsevier, Amsterdam, 2010.
[42] S. Wang, M. Tu, T. Peng, C. Zhang, T. Li, I. Hussain, J. Wang, B. Tan, Porous hypercrosslinked polymer-TiO_2-graphene composite photocatalysts for visible-light-driven CO_2 conversion, Nat. Commun. 10 (2019) 676–686.

[43] B. Li, R. Gong, W. Wang, X. Huang, W. Zhangm, H. Li, C. Hu, B. Tan, A new strategy to microporous polymers: knitting rigid aromatic building blocks by external cross-linker, Macromolecules 4 (2011) 2410–2414.
[44] H.R. Penchah, A. Ghaemi, H.G. Gilani, Benzene-based hyper-cross-linked polymer with enhanced adsorption capacity for CO_2 capture, Energy Fuels 33 (2019) 12578–12586.
[45] L. Ding, H. Gao, F. Xie, W. Li, H. Bai, L. Li, Porosity-Enhanced polymers from hyper-cross-linked polymer precursors, Macromolecules 50 (2017) 956–962.
[46] T. Ratvijitvech, M. Barrow, A.I. Cooper, D.J. Adams, The effect of molecular weight on the porosity of hypercrosslinked polystyrene, Polym. Chem. 6 (2015) 7280–7285.
[47] D. Chen, Y. Fu, W. Yu, G. Yu, C. Pan, Versatile Adamantane-based porous polymers with enhanced microporosity for efficient CO_2 capture and iodine removal, Chem. Eng. J. 334 (2018) 900–906.
[48] M.P. Tsyurupa, V.A. Davankov, Hypercrosslinked polymers: basic principle of preparing the new class of polymeric materials, React. Funct. Polym. 53 (2002) 193–203.
[49] D. Zhang, L. Tao, J. Ju, Y. Wang, Q. Wang, T. Wang, Postmodification of linear poly-p-phenylenes to prepare hyper-crosslinked polymers: tuning the surface areas by the molecular weight, Polymer 60 (2015) 234–240.
[50] V.A. Davankov, S.V. Rogoshin, M.P. Tsyurupa, Macronet isoporous gels through crosslinking of dissolved polystyrene, J. Polym. Sci., Polym. Symp. 47 (1974) 95–101.
[51] V.A. Davankov, M.P. Tsyurupa, Structure and properties of hypercrosslinked polystyrene the first representative of a new class of polymer networks, React. Polym. 13 (1990) 27–42.
[52] D. Fang, X. Li, M. Zou, X. Guo, A. Zhang, Carbazole-functionalized hyper-cross-linked polymers for CO_2 uptake based on Friedel–Crafts polymerization on 9-phenylcarbazole, Beilstein J. Org. Chem. 15 (2019) 2856–2863.
[53] X. Wang, P. Mu, C. Zhang, Y. Chen, J. Zeng, F. Wang, Jia-Xing Jiang, Control synthesis of tubular hyper-cross- linked polymers for highly porous carbon nanotubes, ACS Appl. Mater. Interfaces 9 (2017) 20779–20786.
[54] X. Jiang, Y. Liu, J. Liu, X. Fu, Y. Luo, Y. Lyu, Hypercrosslinked conjugated microporous polymers for carbon capture and energy storage, New J. Chem. 41 (2017) 3915–3919.
[55] Y. Lu, J. Liang, S. Deng, Q. He, S. Deng, Y. Hu, D. Wang, Hypercrosslinked polymers enabled micropore-dominant N, S Co-Doped porous carbon for ultrafast electron/ion transport supercapacitors, Nano Energy 65 (2019) 103993–104001.
[56] S. Pola, C.H. Kuo, W.T. Peng, M.M. Islam, I. Chao, Y.T. Tao, Contorted tetrabenzocoronene derivatives for single crystal field effect transistors: correlation between packing and mobility, Chem. Mater. 24 (2012) 2566–2571.
[57] G. Wang, K. Leus, S. Zhao, P.V.D. Voort, Newly designed covalent triazine framework based on novel N-heteroaromatic building blocks for efficient CO_2 and H_2 capture and storage, ACS Appl. Mater. Interfaces 10 (2018) 1244–1249.
[58] J.Y. Wu, M.G. Mohamed, S.W. Kuo, Directly synthesized nitrogen-doped microporous carbons from polybenzoxazine resins for carbon dioxide capture, Polym. Chem. 8 (2017) 5481–5489.
[59] T. Geng, W. Zhang, Z. Zhu, G. Chen, L. Ma, S. Ye, Q. Niu, A covalent triazine-based framework from tetraphenylthiophene and 2,4,6-trichloro-1,3,5-triazine motifs for sensing o-nitrophenol and effective I_2 uptake, Polym. Chem. 9 (2018) 777–784.
[60] S. Xiong, X. Tang, C. Pan, L. Li, J. Tang, G. Yu, Carbazole-bearing porous organic polymers with a mulberry-like morphology for efficient iodine capture, ACS Appl. Mater. Interfaces 11 (2019) 27335–27342.
[61] X. Zhang, J. Lu, J. Zhang, Porosity enhancement of carbazolic porous organic frameworks using dendritic building blocks for gas storage and separation, Chem. Mater. 26 (2014) 4023–4029.
[62] X. Jing, D. Zou, P. Cui, H. Ren, G. Zhu, Facile synthesis of cost-effective porous aromatic materials with enhanced carbon dioxide uptake, J. Mater. Chem. A 1 (2013) 13926–13931.
[63] R. Dawson, L.A. Stevens, T.C. Drage, C.E. Snape, M.W. Smith, D.J. Adams, A. I. Cooper, Impact of water coadsorption for carbon dioxide capture in microporous polymer sorbents, J. Am. Chem. Soc. 134 (2012) 10741–10744.
[64] S. Yao, X. Yang, M. Yu, Y. Zhang, J.X. Jiang, High surface area hypercrosslinked microporous organic polymer networks based on tetraphenylethylene for CO_2 capture, J. Mater. Chem. A 2 (2014) 8054–8059.
[65] J. Chun, J.H. Park, J. Kim, S.M. Lee, H. Kim, S.U. Son, Tubular-shape evolution of microporous organic networks, Chem. Mater. 24 (2012) 3458–3463.
[66] H. Liu, S. Li, H. Yang, S. Liu, L. Chen, Z. Tang, R. Fu, D. Wu, Stepwise crosslinking: a facile yet versatile conceptual strategy to nanomorphology-persistent porous organic polymers, Adv. Mater. 29 (2017) 1700723–1700731.
[67] G. Liu, Y. Wang, C. Shen, Z. Ju, D. Yuan, A facile synthesis of microporous organic polymers for efficient gas storage and separation, J. Mater. Chem. A 3 (2015) 3051–3058.
[68] G. Shu, C. Zhang, Y. Li, J.X. Jiang, X. Wang, H. Li, F. Wang, Hypercrosslinked silole-containing microporous organic polymers with N-functionalized pore surfaces for gas storage and separation, J. Appl. Polym. Sci. 135 (2018) 45907–45916.
[69] J.G. Li, Y.F. Ho, M.M.M. Ahmed, H.C. Liang, S.W. Kuo, Mesoporous carbons templated by PEO-PCL block copolymers as electrode materials for supercapacitors, Chem. Eur J. 25 (2019) 10456–10463.
[70] J.G. Li, P.Y. Lee, M.M.M. Ahmed, M.G. Mohamed, S.W. Kuo, Varying the hydrogen bonding strength in phenolic/PEO-b-PLA blends provides mesoporous carbons having large accessible pores suitable for energy storage, Macromol. Chem. Phys. 221 (2020), 2000040.
[71] L. Ren, G. Zhang, Z. Yan, L. Kang, H. Xu, F. Shi, Z. Lei, Z.H. Liu, Three-Dimensional tubular MoS2/PANI hybrid electrode for high rate performance supercapacitor, ACS Appl. Mater. Interfaces 7 (2015) 28294–28302.
[72] J. Ping, W. Zhang, P. Yu, H. Pang, M. Zheng, H. Dong, H. Hu, Y. Xiao, Y. Liu, Y. Liang, Improved ion-diffusion performance by engineering an ordered mesoporous shell in hollow carbon nanospheres, Chem. Commun. 56 (2020) 2467–2470.
[73] S. Liu, L. Yao, Y. Lu, X. Hua, J. Liu, Z. Yang, H. Wei, Y. Mai, All-organic covalent organic framework/polyaniline composites as stable electrode for high-performance supercapacitors, Mater. Lett. 236 (2019) 354–357.
[74] C.R. DeBlase, K.E. Silberstein, T.T. Truong, H.D. Abruña, W.R. Dichtel, β-Ketoenamine-linked covalent organic frameworks capable of pseudocapacitive energy storage, J. Am. Chem. Soc. 135 (2013) 16821–16824.
[75] A.F.M. EL-Mahdy, C. Young, J. Kim, J. You, Y. Yamauchi, S.W. Kuo, Hollow microspherical and microtubular [3 + 3] carbazole-based covalent organic frameworks and their gas and energy storage applications, ACS Appl. Mater. Interfaces 11 (2019) 9343–9354.
[76] A.M. Khattak, Z.A. Ghazi, B. Liang, N.A. Khan, A. Iqbal, L. Li, Z. Tang, A redox-active 2D covalent organic framework with pyridine moieties capable of faradaic energy storage, J. Mater. Chem. A 4 (2016) 16312–16317.
[77] Y. Liao, H. Wang, M. Zhu, A. Thomas, Efficient supercapacitor energy storage using conjugated microporous polymer networks synthesized from buchwald–hartwig coupling, Adv. Mater. 30 (2018) 1705710–1705719.
[78] X.C. Li, Y. Zhang, C.Y. Wang, Y.I. Wan, W.Y. Lai, H. Pang, W. Huang, Redox-active triazatruxene-based conjugated microporous polymers for high-performance supercapacitors, Chem. Sci. 8 (2017) 2959–2965.